Spin Hall Effect Transistor
Jörg Wunderlich, *et al.*
Science **330**, 1801 (2010);
DOI: 10.1126/science.1195816

This copy is for your personal, non-commercial use only.

If you wish to distribute this article to others, you can order high-quality copies for your colleagues, clients, or customers by clicking here.

Permission to republish or repurpose articles or portions of articles can be obtained by following the guidelines here.

The following resources related to this article are available online at www.sciencemag.org (this infomation is current as of January 6, 2011):

Updated information and services, including high-resolution figures, can be found in the online version of this article at:
http://www.sciencemag.org/content/330/6012/1801.full.html

Supporting Online Material can be found at:
http://www.sciencemag.org/content/suppl/2010/12/20/330.6012.1801.DC1.html

This article **cites 28 articles**, 4 of which can be accessed free:
http://www.sciencemag.org/content/330/6012/1801.full.html#ref-list-1

This article appears in the following **subject collections:**
Physics, Applied
http://www.sciencemag.org/cgi/collection/app_physics

Downloaded from www.sciencemag.org on January 6, 2011

Science (print ISSN 0036-8075; online ISSN 1095-9203) is published weekly, except the last week in December, by the American Association for the Advancement of Science, 1200 New York Avenue NW, Washington, DC 20005. Copyright 2010 by the American Association for the Advancement of Science; all rights reserved. The title *Science* is a registered trademark of AAAS.

16. D. Gstoehl, A. Brambilla, L. O. Schunk, A. Steinfeld, *J. Mater. Sci.* **43**, 4729 (2008).
17. J. E. Miller *et al.*, *J. Mater. Sci.* **43**, 4714 (2008).
18. C. Perkins, A. W. Weimer, *AIChE J.* **55**, 286 (2009).
19. P. Singh, M. S. Hegde, *Chem. Mater.* **22**, 762 (2010).
20. W. C. Chueh, S. M. Haile, *ChemSusChem* **2**, 735 (2009).
21. W. C. Chueh, S. M. Haile, *Philos. Trans. R. Soc. London Ser. A* **368**, 3269 (2010).
22. S. M. Haile, W. C. Chueh, U.S. Patent application 20,090,107,044 (2009).
23. S. Abanades *et al.*, *J. Mater. Sci.* **45**, 4163 (2010).
24. H. Kaneko *et al.*, *Energy* **32**, 656 (2007).
25. Materials and methods are detailed in supporting material at *Science* Online.
26. C. Li, L. Minh, T. C. Brown, *J. Catal.* **178**, 275 (1998).
27. M. Roeb *et al.*, *Int. J. Hydrogen Energy* **34**, 4537 (2009).
28. Fuel production rate is compared with other thermochemical processes by normalizing the average fuel production rate (as defined in the text) by the mass of the material, including inactive support used to prevent material sintering. The rate for oxygen evolution is not included.
29. G. B. Haxel, J. B. Hedrick, G. J. Orris, "Rare earth elements—Critical resources for high technology" (U.S. Geological Survey Fact Sheet 087-02, Reston, VA, 2002).

30. This work was funded in part by NSF (CBET-0829114), the Initiative for Renewable Energy and the Environment (under subcontract from the University of Minnesota), and the Swiss National Science Foundation (contract no. 200021-126512). Additional travel support was provided by the International Materials Institutes program of NSF under award no. DMR 08-43934. We thank the technical staff of the Solar Technology Laboratory of the Paul Scherrer Institute for supporting the experimental activities at the High-Flux Solar Simulator. W.C.C. designed the experiments, and C.F. designed the solar reactor. Samples were prepared by M.A. and D.S. W.C.C, C.F., P.F., and D.S. executed the experiments. S.M.H. and A.S. supervised the project.

Supporting Online Material
www.sciencemag.org/cgi/content/full/330/6012/1797/DC1
Materials and Methods
Figs. S1 to S3

15 September 2010; accepted 23 November 2010
10.1126/science.1197834

Spin Hall Effect Transistor

Jörg Wunderlich,[1,2]*† Byong-Guk Park,[1]* Andrew C. Irvine,[3]* Liviu P. Zârbo,[2] Eva Rozkotová,[4] Petr Nemec,[4] Vít Novák,[2] Jairo Sinova,[5,2] Tomás Jungwirth[2,6]

The field of semiconductor spintronics explores spin-related quantum relativistic phenomena in solid-state systems. Spin transistors and spin Hall effects have been two separate leading directions of research in this field. We have combined the two directions by realizing an all-semiconductor spin Hall effect transistor. The device uses diffusive transport and operates without electrical current in the active part of the transistor. We demonstrate a spin AND logic function in a semiconductor channel with two gates. Our study shows the utility of the spin Hall effect in a microelectronic device geometry, realizes the spin transistor with electrical detection directly along the gated semiconductor channel, and provides an experimental tool for exploring spin Hall and spin precession phenomena in an electrically tunable semiconductor layer.

Two major themes in semiconductor spintronics research, the spin transistors and the spin Hall effects, have followed distinct and independent scientific paths (*1*, *2*). In the transistor case, the target device concept of a ferromagnetic spin injector and detector connected by a semiconductor channel was established from the outset by Datta and Das (*3*). The ensuing research has focused on the fundamental physical problems related to the resistance mismatch between the transistor's components and to the spin manipulation in the semiconductor via spin-orbit coupling effects (*4*–*15*). By contrast, in the spin Hall effect case, much of the related intriguing quantum-relativistic physics (*16*–*19*) has been established before the first experimental observations (*20*, *21*), but the field is still striving to turn the phenomenon into a concrete device functionality. We demonstrate the applicability of the spin Hall effect in a new type of spin transistor.

The active semiconductor channel in our devices is a two-dimensional electron gas (2DEG) in which the spin-orbit coupling induced spin precession is controlled by external gate electrodes and detection is provided by transverse spin Hall

[1]Hitachi Cambridge Laboratory, Cambridge CB3 0HE, UK. [2]Institute of Physics ASCR, v.v.i., Cukrovarnická 10, 162 53 Praha 6, Czech Republic. [3]Microelectronics Research Centre, Cavendish Laboratory, University of Cambridge, CB3 0HE, UK. [4]Faculty of Mathematics and Physics, Charles University in Prague, Ke Karlovu 3, 121 16 Prague 2, Czech Republic. [5]Department of Physics, Texas A&M University, College Station, TX 77843–4242, USA. [6]School of Physics and Astronomy, University of Nottingham, Nottingham NG7 2RD, UK.

*These authors contributed equally to this work.
†To whom correspondence should be addressed. E-mail: jw526@cam.ac.uk

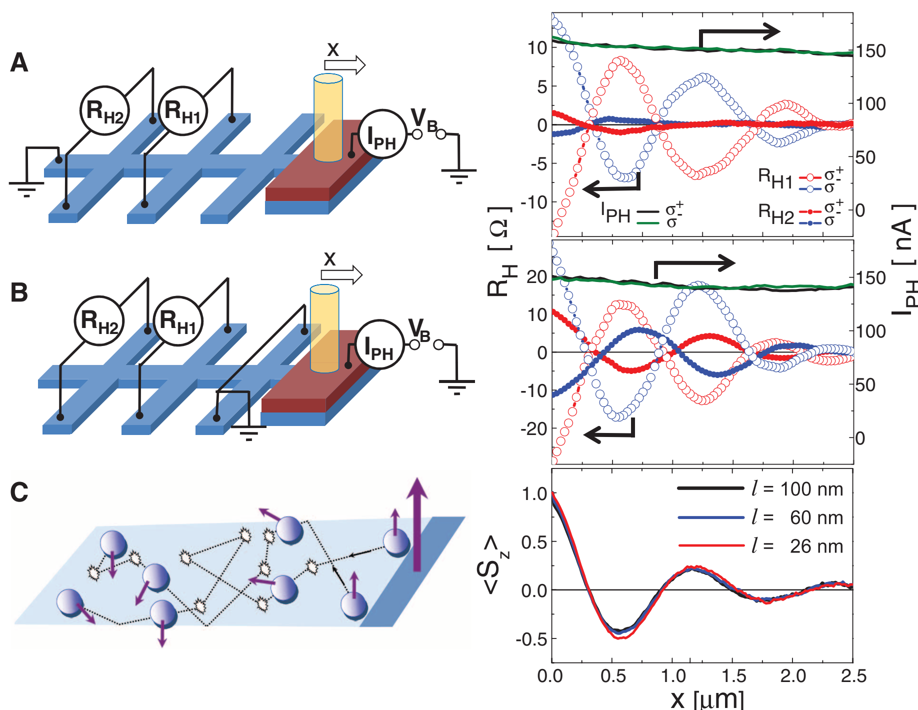

Fig. 1. (**A**) Schematics of the measurement setup with optically injected spin-polarized electrical current propagating through the Hall bar and corresponding experimental Hall effect signals at crosses H1 and H2. The Hall resistances, $R_H = V_H/I_{PH}$, for the two opposite helicities of the incident light are plotted as a function of the focused (~1 μm) light spot position, i.e., of the position of the injection point. Increasing x corresponds to shifting the spot further away from the Hall detectors. (The focused laser beam is indicated by the yellow cylinder in the schematics.) The optical current I_{PH} is independent of the helicity of the incident light and varies only weakly with the light spot position. The applied bias voltage V_B = –15 V, the laser intensity is 1000 W/cm^2, and the laser wavelength is 870 nm. (**B**) Same as (A) for measurement geometry in which electrical current is closed before the first detecting Hall cross H1. (**C**) Schematics of the diffusive transport of injected spin-polarized electrons and Monte-Carlo simulations of the out-of-plane component of the spin of injected electrons averaged over the 1-μm bar cross section assuming Rashba field α = 5.5 meV Å, Dresselhaus field β = –24 meV Å, and different values of the mean free path l.

Downloaded from www.sciencemag.org on January 6, 2011

effect voltages (*22*) measured along the 2DEG Hall bar. For spin injection, we use an optical method described in (*22*) that permits all three components of the spin transistor to be realized within an all-semiconductor structure. The optical injection method is less scalable than electrical injection from ferromagnetic contacts, yet it does not require any magnetic elements or external magnetic fields for the operation of the device. Because of the nondestructive nature of the spin Hall effect detection, one semiconductor channel can accommodate multiple gates and Hall cross detectors and is therefore directly suitable for realizing spin logic operations.

Semiconductor heterostructures used in our experiments, described in detail in (*23*), comprise a modulation p-doped AlGaAs/GaAs heterojunction on top of the structure, 90 nm of intrinsic GaAs, and an n-doped AlGaAs/GaAs heterojunction underneath. In the unetched part of the wafer, the top heterojunction is populated by holes, whereas the 2DEG at the bottom heterojunction is partly depleted. The n-side of the coplanar p-n junction is formed by removing the p-doped surface layer from a part of the wafer, thereby populating the 2DEG. At zero or reverse bias, the device is not conductive in the dark due to charge depletion at the lateral p-n junction. Counterpropagating electron and hole currents can be generated by illumination at subgap wavelengths (*22*). Because of the optical selection rules, the out-of-plane spin polarization of injected electrons is determined by the sense and degree of the circular polarization of vertically incident light.

The n-region is patterned by electron-beam lithography into a 1-μm-wide Hall bar along the $[1\bar{1}0]$ crystallographic axis. The effective width of individual Hall contacts for local spin detection is 50 to 100 nm, and separation between neighboring Hall crosses is 2 μm. Electrical gates controlling the spin currents are placed between one or more pairs of the Hall crosses. The gates are realized by the p-type surface layer areas of the heterostructure, which were locally masked and remained unetched during the fabrication of the n-channel Hall bar (*24*). The laser beam is focused to a ~1- to 2-μm spot at the lateral p-n junction or near the junction on the p-side of the epilayer. For further details on the fabrication of the series of devices used in our study, employed experimental techniques, and the theory of the measured spin-dependent Hall signals, see (*23*). All experimental data presented below were measured at 4 K. As illustrated in (*22*, *23*), our ungated and gated devices operate also at high temperatures.

In Fig. 1, we show experimental results on a control device in which we did not pattern the gate electrodes. These measurements extend previous demonstration of the spin injection Hall effect in similar ungated structures (*22*). In the previous work, we observed that injected spin-polarized electrical currents produce Hall effect signals that are proportional to the out-of-plane component of the local spin polarization. We also demonstrated that spins precess along the channel, resulting in a spatially varying magnitude and sign of the Hall signals on several successive Hall crosses. Because of the limited number of discrete detection points, these experiments did not provide a detailed picture of the spin precession of injected electrons. To better visualize the effect, we use here the optical activity of the device presented in Fig. 1, which extends over a several-micrometer range from the lateral p-n junction into the unetched p-type side of the epilayer. By shifting the focused laser spot, we can smoothly change the position of the spin injection point with respect to the detection Hall crosses. This results in damped oscillatory Hall resistance, $R_H = V_H/I_{PH}$, measured at each of the two successive Hall crosses labeled as H1 and H2 in Fig. 1, placed 6 and 8 μm from the lateral p-n junction. (V_H is the Hall voltage and I_{PH} is the photocurrent.) The oscillations at each Hall cross and the phase shift between signals at the two Hall crosses are consistent with a micrometer-scale spin precession period and with a spin-diffusion length that extends over more than one precession period.

Experiments in Fig. 1 are performed in two distinct electrical measurement configurations. In Fig. 1A, we show data obtained with the source and drain electrodes at the far ends of the p- and n-type sides of the lateral junction, respectively. In this geometry, spin-polarized electrical currents reach the detection Hall crosses, similar to experiments performed in (*22*). In Fig. 1B, the electrical current is drained 4 μm before the first detection Hall cross H1. In this case, only pure spin current (*25*–*27*) reaches crosses H1 and H2. The experiments in Fig. 1 demonstrate that in our 2DEG microchannel, we can realize the Hall effect detection of injected spin-polarized electrical currents, as well as pure spin currents. [For additional measurements of ungated devices, see (*23*).]

The conventional field-effect transistor functionality in our 2DEG channel achieved by the p-layer top gate is demonstrated in Fig. 2A, where we show the gate voltage dependence of the channel current and mobility underneath the gate. At zero gate voltage, we detect only a small residual channel current consistent with the partial depletion of the 2DEG in the unetched part of the heterostructure. By applying forward or reverse voltages of an amplitude less than 1 V, we can open or close the 2DEG channel, respectively, at negligible gate-channel leakage current. Within the range of measurable signals, we detect gate voltage induced changes of the channel current by five orders of magnitude while the mobility changes by two orders of magnitude. The main effect of the gate voltage on the channel current is therefore via direct charge depletion or accumulation of the 2DEG, but mobility changes are also important. With increasing reverse gate voltage, the mobility decreases because the 2DEG is shifted closer to the ionized donors on the other side of the AlGaAs/GaAs heterojunction and because screening of the donor impurity potential by the 2DEG decreases with depletion.

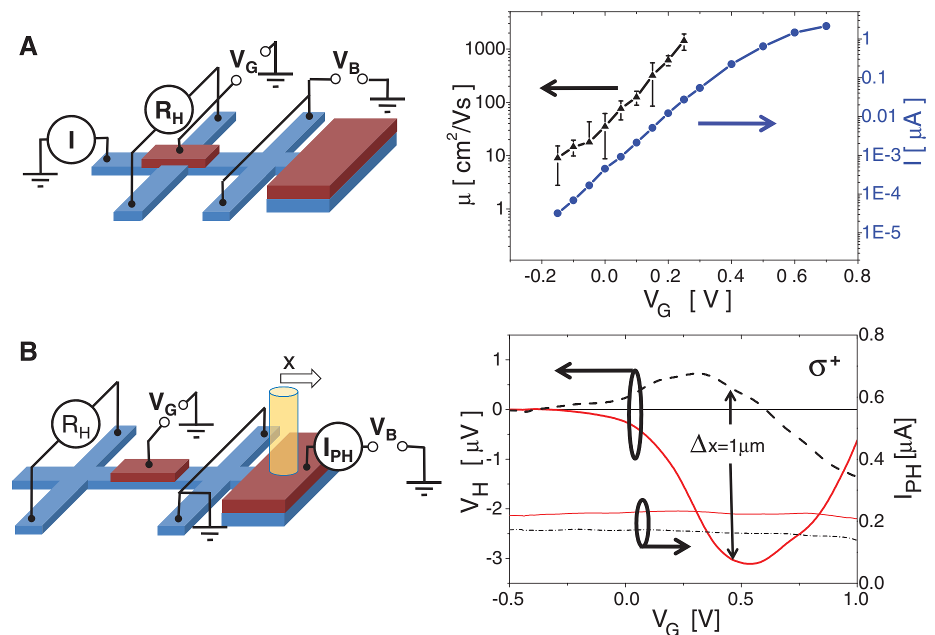

Fig. 2. (**A**) Schematics of the measurement setup corresponding to the conventional field-effect transistor and experimental dependence of the electrical current (blue) through the channel and mobility (black) underneath the gate on the gate voltage. (**B**) Schematics of the setup of the spin Hall transistor and experimental Hall signals as a function of the gate voltage at a Hall cross placed behind the gate electrode for two light spot positions with a relative shift of 1 μm and the dashed black curve corresponding to the spot shifted further away from the detection Hall cross. The applied bias voltage V_B = −10 V, the laser intensity is 700 W/cm^2, and the laser wavelength is 870 nm. The data demonstrate the realization of the spin Hall effect transistor.

Downloaded from www.sciencemag.org on January 6, 2011

The main result of our work (Fig. 2B) is the sensitivity of the measured Hall signal at the cross placed behind the gate on the voltage applied to the gate electrode. To exclude any potential gate voltage dependence of spin-injection conditions in our device, we performed the experiments with the electrical current drained before the gated part of the channel (Fig. 2B). The data show two regimes of operation of our spin transistor. At large reverse voltages, the Hall signals disappear as the diffusion of spin-polarized electrons from the injection region toward the detecting Hall cross is blocked by the repulsive potential of the intervening gate electrode. Upon opening the gate, the Hall signal first increases, in analogy to the operation of the conventional field-effect transistor. We emphasize, however, that while the optically generated current I_{PH} is kept constant, the electrical current in our experiments in the manipulation and detection parts of the transistor channel remains zero at all gate voltages. The onset of the output transverse electrical signal upon opening the gate is a result of a pure spin current. The mechanism by which the spin current generates the output signal cannot be ascribed to a normal charge Hall effect because of the absence of magnetic field and charge current underneath the cross.

The initial increase of the detected output signal upon opening the gate is followed by a non-monotonic gate voltage dependence of the Hall voltage (Fig. 2B). This is in marked contrast to the monotonic increase of the normal electrical current in the channel observed in the conventional field-effect transistor measurement in Fig. 2A. Apart from blocking the spin current at large reverse gate voltages, the intermediate gate electric fields are modifying spin precession of the injected electrons and therefore the local spin polarization at the detecting Hall cross when the channel is open. This is the spin manipulation regime analogous to the original Datta-Das proposal of a spin transistor. We further demonstrated the presence of this regime in our device by comparing two measurements shown in Fig. 2B: one where the laser spot is aligned close to the lateral p-n junction on the p-side (red solid line), and the other with the spot shifted by ~1 μm in the direction away from the detecting Hall crosses (black dashed line). The reverse voltage at which the Hall signals disappear is the same in the two measurements. For gate voltages at which the channel is open, the signals are shifted with respect to each other in the two measurements and have opposite sign at certain gate voltages, and the overall magnitude of the signal is larger for smaller separation between injection and detection points, all confirming the spin precession origin of the observed effect. [For additional measurements of gated devices see (*23*).]

One of the important attributes of our nondestructive spin detection method integrated, together with the electrical spin manipulation, along the semiconductor channel is the possibility of fabricating devices with a series of Hall cross detectors and also with a series of gates. In Fig. 3, we demonstrate the feasibility of this concept and of the ensuing logic functionality on a spin Hall effect transistor structure with two gates, the first placed before cross H1 and the second before H2. The scanning electron micrograph of the device is shown in Fig. 3A. The measured data plotted in Fig. 3B demonstrate that Hall cross H1 responds strongly to the electric field on the first gate, with gate voltage characteristics similar to those observed in the single-gate device in Fig. 2. As expected for the relative positions of the injection point, of Hall cross H1, and of the two gates in the device, the dependence of the signal at cross H1 on the second gate is much weaker. By contrast, Hall cross H2 responds strongly to both gates (Fig. 3C). Before the spin can reach the detecting Hall cross H2, it is manipulated by two external parameters. This is analogous to the measurement in Fig. 2B in which the position of the injection point played the role of the second parameter. The analogy between results in Figs. 2B and 3C further demonstrates the spin origin of the functionality of our transistor structures.

In Fig. 3D we demonstrate a simple AND logic functionality by operating both gates and by measuring the Hall electrical signal at cross H2. Intermediate gate voltages on both gates represent the input value 1 and give the largest electrical signal at H2 (positive for σ^- helicity of the incident light), representing the output value 1. When we apply to any of the two gates a large reverse (negative) gate voltage, representing input 0, the electrical signal at H2 disappears, i.e., the output is 0. Note that additional information is contained in the polarization dependence of the detected Hall signals, as illustrated in Fig. 3D.

Proceeding to the theoretical analysis of the measured data, we first characterize the transport regime in which our devices operate. The 2DEG mobilities in the etched, n-type part of the wafer and underneath the p-layer gates are $\lesssim 3 \times 10^3$ cm^2/Vs, corresponding to a mean-free path $\lesssim 10^2$ nm. This is much smaller than the precession length and the length of our 2DEG channel, i.e., the experiments are done in the diffusive, strong-disorder weak spin-orbit coupling regime. As explained in (*22*), the Hall effect and the spin-precession effect can be decoupled in this regime. The Hall effect measures the local out-of-plane component of the spin polarization of carriers and originates from the spin-orbit coupling induced skew scattering. [See (*23*) for quantitative estimates of the Hall signals that are consistent with experiment.] In the following analysis, we

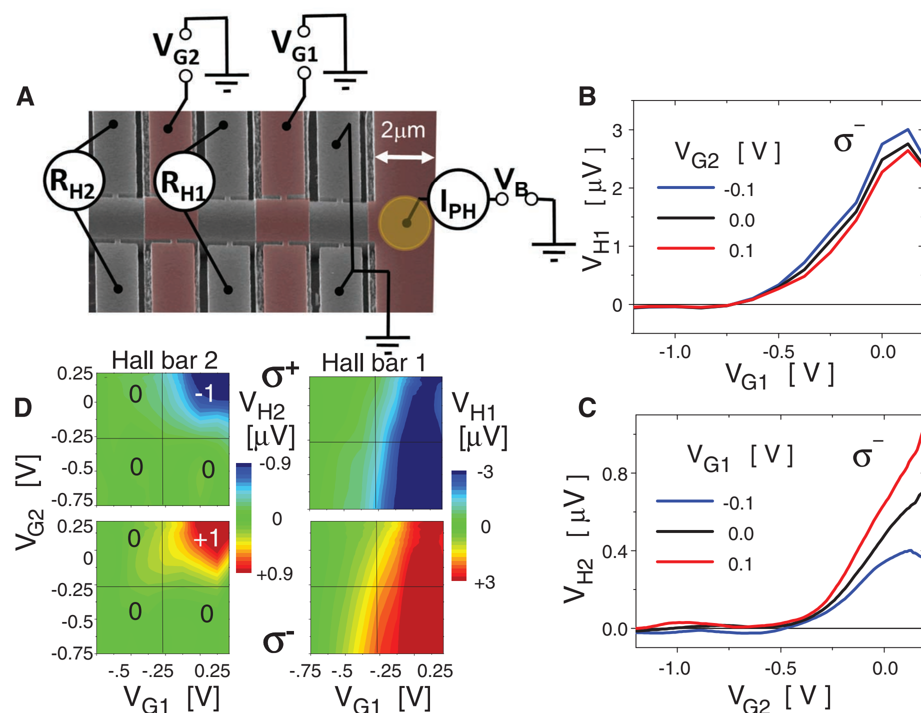

Fig. 3. (**A**) Scanning electron micrograph and schematics of the device with two detecting Hall crosses H1 and H2 and one gate placed before cross H1 and the second gate placed behind cross H1 and before cross H2. Gates and p-side of the lateral p-n junction are highlighted in red. The focused laser beam is indicated by the yellow spot. (**B**) Hall signals at cross H1 measured as a function of the first gate voltage. These gating characteristics are similar to those of the single-gate device in Fig. 2B and have much weaker dependence on the second gate voltage. (**C**) Hall signals at cross H2 measured as a function of the second gate voltage. The curves show strong dependence on the voltages on both gates. (**D**) Demonstration of the spin AND logic function by operating both gates (input signals) and measuring the response at Hall cross H2 (output signal). Measured data at cross H1 are also shown for completeness. The applied bias voltage $V_B = -10$ V, the laser intensity is 400 W/cm^2, and the laser wavelength is 870 nm.

Downloaded from www.sciencemag.org on January 6, 2011

focus on the spin-precession and spin-diffusion lengths. The possibility of observing and using spin precession of an ensemble of electrons in the diffusive regime is demonstrated by our numerical Monte Carlo simulations (*22*, *28*) shown in Fig. 1C.

The numerically obtained spin-precession period is well described by an analytical formula derived from the dynamics of the spin-density matrix (*28*), $L_{SO} = \pi\hbar^2/m^*(|\alpha| + |\beta|)$; $m^* = 0.067$ is the electron effective mass in GaAs. There are two regimes in which spin precession can be observed in the diffusive transport regime. In one regime, the width of the channel is not relevant and a spin-diffusion length larger than the precession length occurs as a result of the single-particle transport analog of the spin helix state (*9*) realized at 2DEG Rashba and Dresselhaus spin-orbit fields of equal or similar strengths, $\alpha \approx -\beta$ for our bar orientation. When the two spin-orbit fields are not tuned to similar strengths, the spin-diffusion length is approximately given by $\sim L_{SO}^2/w$ and spin precession is therefore observable only when the width w of the channel is comparable to or smaller than the precession length (*28*–*30*).

The complex design of our semiconductor heterostructure provides simultaneously the means for spin injection, electrical gating, and detection, so we did not rely on further fine tuning of the internal spin-orbit fields to realize the spin helix state condition. Instead, we fabricated narrow Hall bars whose width is smaller than the precession length and used a strongly focused light spot for spin injection. As shown in Fig. 1C, several precessions are readily observable in this quasi one-dimensional geometry even in the diffusive regime and for $\alpha \neq -\beta$, and the spin-precession and spin-diffusion lengths in this regime are independent of the mean-free-path, i.e., of the mobility of the 2DEG channel (*28*).

The strength of the confining electric field of the 2DEG underneath the gate changes by up to a factor of ~2 in the range of applied gate voltages in our experiments. This result implies (*22*) comparably large changes in the strength of the internal spin-orbit fields in the 2DEG channel. The dependence on the spin-orbit field strength shown in the above equation and confirmed by Monte Carlo simulations (*28*) (and the independence on the momentum of injected electrons) implies also comparably large changes in the spin-precession length. These estimates corroborate the observed spin manipulation in our spin Hall effect transistors by external electric fields applied to the gates.

References and Notes

1. I. Žutić, J. Fabian, S. Das Sarma, *Rev. Mod. Phys.* **76**, 323 (2004).
2. T. Dietl, D. D. Awschalom, M. Kaminska, H. Ohno, Eds., *Spintronics*, vol. 82 of *Semiconductors and Semimetals* (Elsevier, Amsterdam, 2008).
3. S. Datta, B. Das, *Appl. Phys. Lett.* **56**, 665 (1990).
4. J. M. Kikkawa, D. D. Awschalom, *Nature* **397**, 139 (1999).
5. H. J. Zhu *et al.*, *Phys. Rev. Lett.* **87**, 016601 (2001).
6. P. R. Hammar, M. Johnson, *Phys. Rev. Lett.* **88**, 066806 (2002).
7. G. Schmidt, L. W. Molenkamp, *Semicond. Sci. Technol.* **17**, 310 (2002).
8. J. Schliemann, J. C. Egues, D. Loss, *Phys. Rev. Lett.* **90**, 146801 (2003).
9. B. A. Bernevig, J. Orenstein, S.-C. Zhang, *Phys. Rev. Lett.* **97**, 236601 (2006).
10. X. Jiang *et al.*, *Phys. Rev. Lett.* **94**, 056601 (2005).
11. S. A. Crooker *et al.*, *Science* **309**, 2191 (2005).
12. C. P. Weber *et al.*, *Phys. Rev. Lett.* **98**, 076604 (2007).
13. X. Lou *et al.*, *Nat. Phys.* **3**, 197 (2007).
14. B. Huang, D. J. Monsma, I. Appelbaum, *Phys. Rev. Lett.* **99**, 177209 (2007).
15. H. C. Koo *et al.*, *Science* **325**, 1515 (2009).
16. M. I. Dyakonov, V. I. Perel, *Phys. Lett. A* **35**, 459 (1971).
17. J. E. Hirsch, *Phys. Rev. Lett.* **83**, 1834 (1999).
18. S. Murakami, N. Nagaosa, S.-C. Zhang, *Science* **301**, 1348 (2003).
19. J. Sinova *et al.*, *Phys. Rev. Lett.* **92**, 126603 (2004).
20. Y. K. Kato, R. C. Myers, A. C. Gossard, D. D. Awschalom, *Science* **306**, 1910 (2004).
21. J. Wunderlich, B. Kaestner, J. Sinova, T. Jungwirth, *Phys. Rev. Lett.* **94**, 047204 (2005).
22. J. Wunderlich *et al.*, *Nat. Phys.* **5**, 675 (2009).
23. Materials and methods are available on *Science* online.
24. B. Kaestner, J. Wunderlich, T. J. B. M. Janssen, *J. Mod. Opt.* **54**, 431 (2007).
25. S. O. Valenzuela, M. Tinkham, *Nature* **442**, 176 (2006).
26. C. Brüne *et al.*, *Nat. Phys.* **6**, 448 (2010).
27. E. S. Garlid, Q. O. Hu, M. K. Chan, C. J. Palmstrøm, P. A. Crowell, *Phys. Rev. Lett.* **105**, 156602 (2010).
28. L. P. Zârbo, J. Sinova, I. Knezevic, J. Wunderlich, T. Jungwirth, *Phys. Rev. B* **82**, 205320 (2010).
29. A. A. Kiselev, K. W. Kim, *Phys. Rev. B* **61**, 13115 (2000).
30. S. Kettemann, *Phys. Rev. Lett.* **98**, 176808 (2007).

31. We acknowledge support from European Union grant FP7-215368 SemiSpinNet; Czech Republic grants AV0Z10100521, MSM0021620834, KAN400100652, LC510, and Preamium Academiae; and U.S. grants NSF-MRSEC DMR-0820414, ONR-N000140610122, DMR-0547875, and SWAN-NRI. J.S. is a Cottrell Scholar of Research Corporation. In connection with this work, we have two pending patent applications with the European Patent Office, patent numbers EP 2 224 500 A2 and EP 2 190 022 A.

Supporting Online Material

www.sciencemag.org/cgi/content/full/330/6012/1801/DC1
Materials and Methods
SOM Text
Figs. S1 to S10
Table S1
References

29 July 2010; accepted 22 November 2010
10.1126/science.1195816

Brownian Motion of Stiff Filaments in a Crowded Environment

Nikta Fakhri,[1] Frederick C. MacKintosh,[2] Brahim Lounis,[3] Laurent Cognet,[3] Matteo Pasquali[1]*

The thermal motion of stiff filaments in a crowded environment is highly constrained and anisotropic; it underlies the behavior of such disparate systems as polymer materials, nanocomposites, and the cell cytoskeleton. Despite decades of theoretical study, the fundamental dynamics of such systems remains a mystery. Using near-infrared video microscopy, we studied the thermal diffusion of individual single-walled carbon nanotubes (SWNTs) confined in porous agarose networks. We found that even a small bending flexibility of SWNTs strongly enhances their motion: The rotational diffusion constant is proportional to the filament-bending compliance and is independent of the network pore size. The interplay between crowding and thermal bending implies that the notion of a filament's stiffness depends on its confinement. Moreover, the mobility of SWNTs and other inclusions can be controlled by tailoring their stiffness.

Crowding greatly constrains the transversal mobility of a filament and causes anisotropic diffusion, which is limited to the filament axial direction. In the case of polymer solutions or melts, understanding the motion of a single polymer chain confined by the meshwork of its neighbors was key to a number of advances in polymer science. In their seminal work, de Gennes, Doi, and Edwards (*1*–*3*) modeled the effect of crowding on polymer dynamics by introducing the concept of a confining tube, together with preferential motion along the polymer's axis, known as reptation because of its resemblance to the slithering of a snake (Fig. 1A, inset). This model captured many bulk dynamical properties of flexible polymer melts and solutions (*4*), although direct experimental evidence validating this powerful theoretical intuition came over two decades later, when reptation of flexible and semi-flexible filaments was observed directly by imaging fluorescently labeled DNA (*5*) and actin (*6*).

In contrast, little is known about the thermal motion of stiff filaments such as carbon nanotubes, biopolymers, and stiff fibers in a network. In particular, the role of the bending stiffness of such inclusions remains controversial, with long-standing conflicting theoretical predictions (*7*–*11*). Doi predicted that rotational diffusion is independent of stiffness (*7*), whereas Odijk concluded that such diffusion should be enhanced by flexibility (*9*) and Sato concluded the opposite (*11*). Bulk experiments by means of birefringence and dichroism (*12*–*14*) have also given conflicting

[1]Department of Chemical and Biomolecular Engineering, Department of Chemistry, Smalley Institute for Nanoscale Science and Technology, Rice University, Houston, TX 77005, USA. [2]Department of Physics and Astronomy, Vrije Universiteit, 1081 HV Amsterdam, Netherlands. [3]Centre de Physique Moléculaire Optique et Hertzienne, Université de Bordeaux CNRS, Talence F-33405, France.

*To whom correspondence should be addressed. E-mail: mp@rice.edu

Downloaded from www.sciencemag.org on January 6, 2011